BATTERIES

Self-heating–induced healing of lithium dendrites

Lu Li,[1] Swastik Basu,[1] Yiping Wang,[2] Zhizhong Chen,[2] Prateek Hundekar,[1,2] Baiwei Wang,[2] Jian Shi,[2] Yunfeng Shi,[2] Shankar Narayanan,[1] Nikhil Koratkar[1,2]*

Lithium (Li) metal electrodes are not deployable in rechargeable batteries because electrochemical plating and stripping invariably leads to growth of dendrites that reduce coulombic efficiency and eventually short the battery. It is generally accepted that the dendrite problem is exacerbated at high current densities. Here, we report a regime for dendrite evolution in which the reverse is true. In our experiments, we found that when the plating and stripping current density is raised above ~9 milliamperes per square centimeter, there is substantial self-heating of the dendrites, which triggers extensive surface migration of Li. This surface diffusion heals the dendrites and smoothens the Li metal surface. We show that repeated doses of high-current-density healing treatment enables the safe cycling of Li-sulfur batteries with high coulombic efficiency.

The demand for higher-energy-density battery systems (*1*, *2*) has created a renewed interest in the exploration of metallic lithium (Li) as an anode material. This is because the packing density of Li atoms is the highest in its metallic form, resulting in an ultrahigh (*3*) theoretical specific capacity of 3861 mAh g^{-1}. However, the main stumbling block to deployment of Li metal anodes is the nucleation and growth of "dendritic" projections (*4*, *5*) during the electrochemical plating-stripping process that occurs when the battery is being charged or discharged. These Li dendrites are problematic in many respects. They increase irreversible capacity loss, reduce the coulombic efficiency (CE), and promote the degradation and drying of the electrolyte (*6*, *7*). However, the most pressing issue is that the sharp dendritic projections can pierce through the battery separator and electrically short the battery (*8*–*10*). This results in a severe thermal runaway situation, which could result in the battery catching fire.

Researchers have over the years devised various innovative approaches (*11*–*17*) to control and suppress the growth of Li dendrites, but 100% suppression is challenging. This is because kinetically, the nucleation and growth of Li dendrites is highly favorable during electrochemical plating and stripping reactions. In general, it is taken for granted that higher current densities in a Li metal battery will yield accelerated growth of dendrites. In this Report, we demonstrate a distinct regime for Li dendrite evolution in which the opposite holds true. For our battery system, we found that when the plating-stripping current density is raised above ~9 mA cm^{-2}, there is substantial self-heating of the dendrites. The local heating gives flux and flow to Li, triggering extensive surface diffusion, which smoothens the dendrites and enables the equilibrium flat configuration to be established quicker. The self-heating is at safe levels, below any danger of electrolyte breakdown or thermal damage to the separator.

To elucidate the underlying science behind the dendrite healing, we tested Li-Li symmetric cells (fig. S1A). The tests were performed over a wide range of operating current densities, ranging from low (~0.75 mA cm^{-2}) to very high values (~15 mA cm^{-2}). The potential-time and current-time profiles during galvanostatic charge-discharge cycling in Li-Li symmetric cells under different current densities are shown in fig. S1, D and E. In the ideal thermodynamic condition, the voltage of Li stripping and plating should be at 0 V (versus Li-Li^+). However, in practice an overpotential exists, which increases substantially with the operating current density (figs. S1, D and E, and S2). Electrochemical impedance spectra (EIS) of the Li-Li symmetric cells were recorded before and after 50 charge-discharge cycles at different current densities, and the results are summarized in fig. S1, B and C. A striking observation is that the electrolyte resistance of the Li-Li symmetrical cell cycled at ~15 mA cm^{-2} remains ~8 ohms both before and after 50 cycles, whereas the corresponding resistance of the cell cycled at ~0.75 mA cm^{-2} increases by ~75% from ~10 ohms before cycling to ~17.5 ohms after only 50 charge-discharge steps. The rapid increase in electrolyte resistance observed in fig. S1, B and C, is a signature of dendritic growth. The continuous formation of solid electrolyte interface (SEI) on the proliferating dendrites will cause electrolyte drying, which increases the resistance to Li^+ transport. The electrochemical evidence in fig. S1, B and C, therefore suggests that Li dendrite nucleation and growth appears to flourish at current densities of ~0.75 mA cm^{-2}, whereas it seems to be suppressed when the cell is operated at current densities of ~15 mA cm^{-2}, an order of magnitude higher.

To corroborate the electrochemical evidence, we carried out ex situ scanning electron microscopy (SEM) imaging of the surfaces of the Li metal foils used in the experiments. Before cycling, the Li foils displayed a relatively smooth appearance and were completely free of dendrites (fig. S3). Shown in Fig. 1, A to D, are SEM images of the Li metal electrode surface after 50 cycles of charge and discharge at current densities of ~0.75, ~4.5, ~9.0, and ~15 mA cm^{-2}. Under low current density (~0.75 mA cm^{-2}) (Fig. 1A), a few isolated but large-diameter dendritic particles can be observed. With the increase of current density (Fig. 1B), the diameter of Li dendrites decreases, but the packing density of the protrusions has increased substantially. However, when the current density was increased all the way up to ~15 mA cm^{-2} (Fig. 1D), the dendrites tend to fuse (merge) together. As a consequence, the surface of the Li electrode becomes much smoother, which substantially lowers the risk of dendrite penetration through the separator. At an intermediate current density of ~9 mA cm^{-2}, there is partial healing (Fig. 1C) of dendrites. This was also corroborated with cross-sectional SEM imaging of the Li metal foils (Fig. 1, E to H). As the current density is raised from ~0.75 to ~9 mA cm^{-2}, the dendritic layer becomes more prominent, increasing in thickness from ~14 to ~37% of the Li foil thickness. However, at ~15 mA cm^{-2} current density the dendritic layer undergoes a striking transformation. The dendrites fuse through the entire thickness of the dendritic layer (~48% of the Li foil thickness), transforming into a relatively smooth and compact (dense) layer.

High-magnification SEM images of the dendrite particles in Fig. 1 are provided in fig. S4. Direct microscopy evidence for fusing of the dendrites is provided in fig. S5. X-ray diffraction (XRD) and Raman spectroscopy confirms that these particles are Li dendrites and not surface contaminants (figs. S6 and S7). SEI compositional analysis indicates that the material composition of the SEI is similar over a wide range of current densities (fig. S8). To verify that electrical shorting is suppressed in cells with the healed Li surface, we performed extended cycling of the Li-Li symmetrical cells (fig. S9). We found that at the lower current densities (such as ~4.5 mA cm^{-2}), the Li-Li cell shorts in ~500 hours because of the dendritic projections that develop on the surfaces of the Li electrodes. By contrast, cells that were cycled at ~15 mA cm^{-2} showed no indication of electrical shorting even after 2000 hours (fig. S9).

To obtain a better understanding of the dendrite nucleation and growth process, in situ observation was carried out by using an optical microscope (figs. S10 and S11). As shown in fig. S11, when different current densities are applied, distinct nucleation patterns emerge. When low current density (fig. S11, A to D) is applied, there are almost no dendrite nuclei observed on the Li electrode in the initial 20 min. At further times, several large Li nuclei gradually arise

[1]Department of Mechanical, Aerospace and Nuclear Engineering, Rensselaer Polytechnic Institute, Troy, NY 12180, USA. [2]Department of Material Science and Engineering, Rensselaer Polytechnic Institute, Troy, NY 12180, USA.
*Corresponding author. Email: koratn@rpi.edu

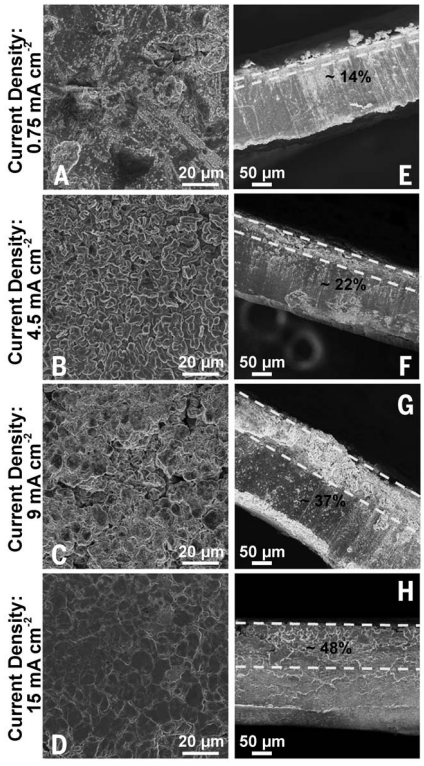

Fig. 1. Morphology evolution of Li dendrites in Li-Li symmetrical cells under different current densities. (**A** and **E**) ~0.75 mA cm^{-2}. (**B** and **F**) ~4.5 mA cm^{-2}. (**C** and **G**) ~9 mA cm^{-2}. (**D** and **H**) ~15 mA cm^{-2}.

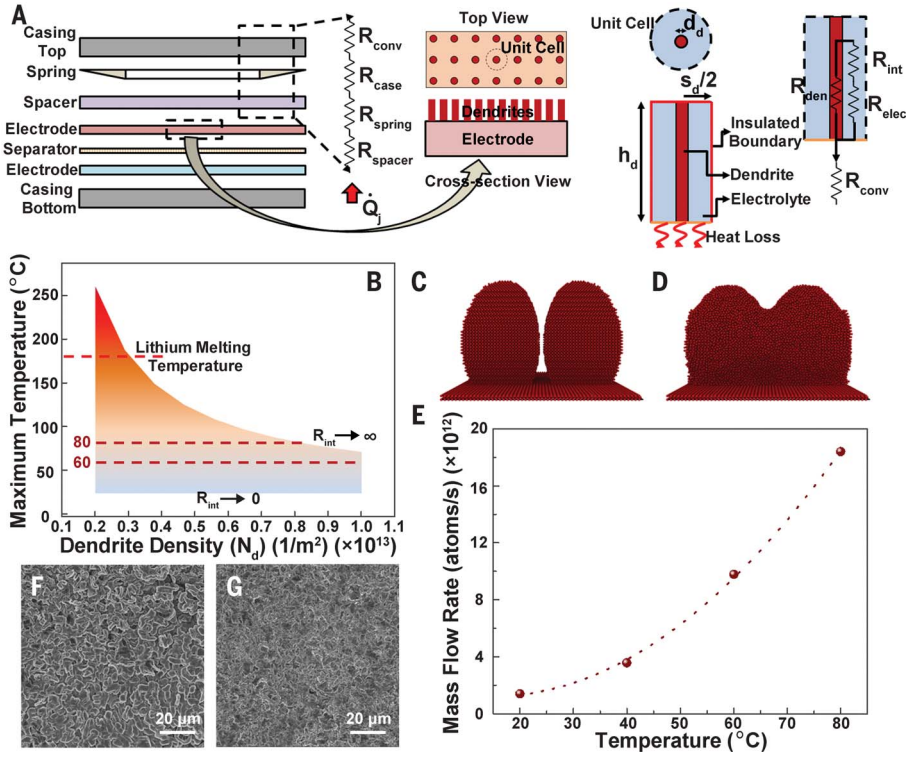

Fig. 2. Dendrite healing mechanism. (**A**) Cross-section diagram of the coin cell. Because of a repetitive geometry, a unit cell is used for thermal modeling of a single dendrite with characteristic diameter (d_d), height (h_d), and spacing (s_d). As shown in the resistance diagram, heat generated in the dendrite can either be conducted to the substrate directly or via the surrounding electrolyte. R_{conv}, R_{case}, R_{spring}, and R_{spacer} denote thermal resistances to heat transfer, corresponding to natural convection, casing, spring and spacer, respectively. R_{den}, R_{elec}, and R_{int} denote thermal resistances to heat transfer, corresponding to the dendrite, electrolyte and their interface, respectively. (**B**) Maximum dendrite temperatures at a current density of ~15 mA cm^{-2}. For the typical range of interfacial thermal resistances, dendrite temperatures in the range of 60 to 80°C are predicted. (**C** and **D**) Screenshots of molecular models used in MD simulation, (C) initial state and (D) after ~50 ps at ~80°C. (**E**) Migration mass flow rate of Li atoms at different temperatures as predicted with MD. (**F**) SEM image of Li dendrites in Li-Li symmetrical cells operated at a current density of ~4.5 mA cm^{-2} for 50 charge-discharge cycles. (**G**) Healing of the dendrites in (F) by means of thermal annealing in an inert Ar environment at ~70°C for 3 days.

but are well spaced apart. In contrast to this, at high current density (fig. S11, E to H), densely packed dendritic nuclei (dark spots) spring out over the entire Li electrode surface within just a few minutes. Additional microscopy evidence of finer and densely populated dendrites at higher current densities is provided in fig. S12. We used classical nucleation and growth theory to model this phenomenon (supplementary text). The predictions (fig. S11K) indicate that the electrochemical over-potential increases with increase in the current density. This higher over-potential reduces the nucleation radius and increases the nucleation rate and the nucleation site density of the dendrites (fig. S11, J and L). The dense-packing of dendrites implies that the majority of the current must collectively flow through the dendrites to reach the Li electrode. The resulting Joule heating of the dendrites could trigger extensive surface diffusion of Li, enabling the closely packed dendritic particles to be fused together. In addition to high packing density, the large over-potentials also generate finer dendrites, which in conjunction with the high current density should generate substantial self (Joule) heating.

To evaluate the temperature rise in the dendrites, we carried out detailed heat transfer simulations (Fig. 2A and supplementary text). We found that the predicted temperature rise (Fig. 2B) in the dendrites at current densities of ~15 mA cm^{-2} are on the order of 40 to 60°C. The electrolyte and membrane separator (*18*) used in our experiments did not degrade at these temperatures. Our thermal model indicates that even such moderate temperature increases are not feasible at low current densities (such as ~0.75 mA cm^{-2}) (fig. S13). Although temperature increases on the order of 40 to 60°C are clearly not large enough to melt dendrites (the melting temperature of Li is ~180.5°C, and the dendrites are large enough to rule out any size effect on the melting temperature), they may be sufficiently high to promote diffusion of Li atoms on the dendritic surfaces. To investigate this, we carried out molecular dynamics (MD) simulations of the Li diffusion process at various temperatures from room temperature (20°C) to 80°C (temperature rise of ~60°C). The molecular model and arrangement of the Li dendrite particles used in our simulation is shown in Fig. 2C. To quantitatively assess the mass transport as a function of temperature, we focused on the atom migration from the dendrite surface to the valley formed between two neighboring dendrite particles. The results for the migration mass flow rate (atoms per second) of Li atoms as a function of temperature is shown in Fig. 2E. Because the driving force for surface migration is essentially the difference in chemical potential because of curvature (very similar to Ostwald ripening), a nonzero flux was observed even at room temperature. However, the surface diffusion of Li is strongly temperature-dependent, with a sharp increase in the migration mass flow rate above 40°C. Shown in Fig. 2D is the MD prediction for the morphology of the dendritic particles after annealing at ~80°C for ~50 ps. We clearly observed merging and fusing of the dendrite particles, which is consistent with our experimental observations. Although the time scales in the MD simulations are very different from the experiments, the essential physics remain the same.

To confirm that the healing is a thermal effect, we carried out a dendrite annealing control experiment. In this test, a Li-Li symmetrical cell

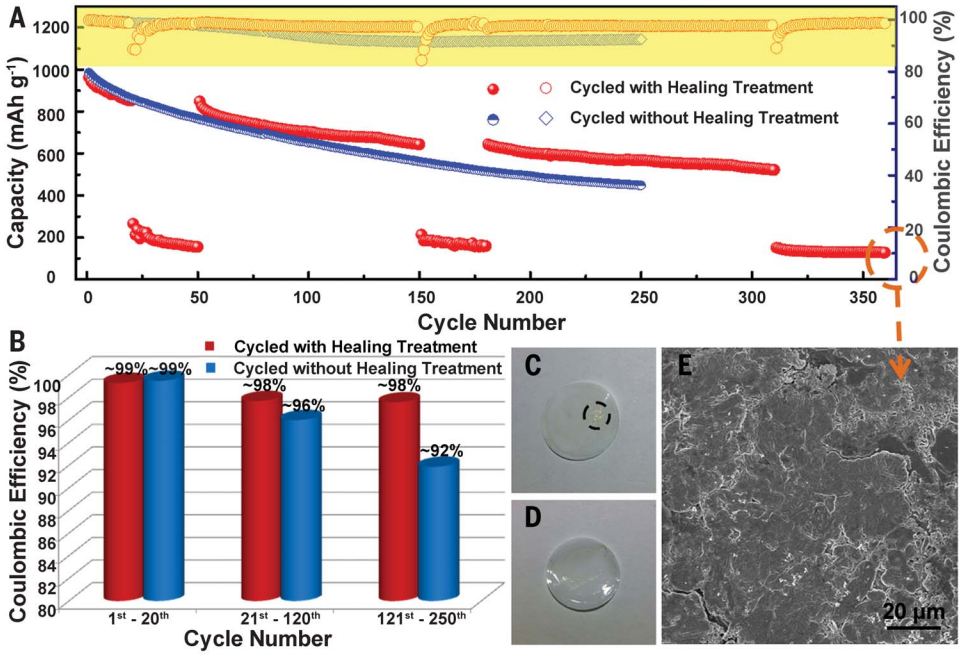

Fig. 3. Dendrite healing in a Li-S battery. (**A**) Cycle stability and CE (highlighted in yellow) of Li-S batteries with and without periodic doses of healing treatment. Blue data points indicate performance of the baseline Li-S cell cycled at ~0.75 mA cm^{-2} without healing treatment. The red data points are for intermittent healing treatment (at current density of ~9 mA cm^{-2}) applied between the 21st and 50th, 151st and 180th, and 311th and 360th cycles. For the remaining cycles, a current density of ~0.75 mA cm^{-2} was applied, which is identical to the baseline cell without healing. (**B**) Comparison of average CE of the Li-S battery when operated at a current density of ~0.75 mA cm^{-2} with and without the healing treatment. (**C**) Digital photo of membrane separator in the cycled Li-S batteries after 250 cycles of charge-discharge at a current density of ~0.75 mA cm^{-2} without the healing treatment. The dashed circle indicates the presence of dendritic Li particles that are impregnated in the separator. (**D**) Corresponding photo of the membrane separator taken after 360 cycles of charge-discharge with the healing treatment. (**E**) Morphology of the Li metal electrode surface after the third healing stage [after the 360th charge-discharge cycle indicated in (A) by the dashed circle].

was cycled at a current density of ~4.5 mA/cm^2 for 50 charge-discharge cycles (~200 hours). Then, the cell was thermally annealed at a temperature of ~70°C for ~3 days. SEM images of the Li metal electrode before and after annealing are shown in Fig. 2, F and G, respectively. The annealed Li foil displays a relatively smooth film-like morphology, similar to the electrochemically tested Li foils that were cycled at high current densities (Fig. 1D). To eliminate the possibility that pressure buildup in a closed coin cell contributes to the healing, we also performed an annealing experiment in an open-cell configuration. For this test, a Li-Li cell was cycled at ~4.5 mA/cm^2 for 50 charge-discharge steps in order to form the dendrites. Then the cell was opened in an inert argon (Ar) environment, inside a glove box. The Li foil was removed from the cell and placed on a hot plate (within the glove box) and thermally annealed at ~70°C for ~3 days. Similar to the closed-cell case, SEM imaging (after annealing) of the Li foil in the open-cell configuration also revealed a relatively smooth surface (fig. S14), indicating healing of the dendrites.

We investigated the grain size distribution of the Li dendrites based on image analysis of Fig. 1, B and D. At moderately large current densities (~4.5 mA cm^{-2}), the average grain sizes are ~5.7 ± 2 μm along the longest dimensions and ~2.7 ± 0.7 μm along the shortest dimensions (fig. S15). However, at ultrahigh current densities (~15 mA cm^{-2}), it is evident that the dendrite morphology has changed because the grains get much larger—~8.8 ± 3 μm along the longest dimensions and ~5.2 ± 2 μm along the shortest dimensions—and are more broadly distributed (fig. S15). These results are consistent with the picture of surface diffusion–driven dissolution and merging (coarsening) of the dendrites. Because the high current density is applied during both plating and stripping, we expected the healing to occur during both the plating and stripping step. This was corroborated by a comparison of the Li foils after plating and stripping at a current density of ~15 mA cm^{-2} (fig. S16), indicating a similar (flat) morphology with comparable grain sizes.

So far, we have reported dendrite healing in Li-Li symmetrical cells. The question remained whether such effects can be reproduced in practical situations. To study this, we tested a Li-sulfur (Li-S) full cell (fig. S17A) (*19*). For this configuration, the anode is a Li metal foil, whereas the cathode is a S-carbon composite (*18*). Unlike Li-Li symmetrical cells, for Li-S batteries, even under a low current density (~0.75 mA cm^{-2}), the Li dendrites are densely packed (fig. S17D). This can be understood from the voltage profile for the Li-S battery (fig. S17B). On the basis of the thermodynamics of the Li anode and sulfur cathode, the electrochemical reaction (*20*) takes place at ~2 V. Because of this large over-potential (related to Li plating and stripping), the dendrites are densely packed irrespective of the current density at which the cell is operated. Of course, current densities of ~0.75 mA cm^{-2} are insufficient to heal the dendrites through Joule heating; however, when we increased the current density to ~9.0 mA cm^{-2}, we clearly observed healing of the dendrites into a relatively smooth (film-like) morphology (fig. S17E). The galvanostatic charge-discharge cycling and CE results for the Li-S battery are provided in fig. S17C. A key indicator of the severity of dendrites is low CE; as indicated in fig. S17C, the CE of the cell cycled under high current density is close to 100%, whereas the CE is continuously decreasing when the cell is cycled at low current density. To demonstrate that the healing mechanism in this case is identical to the previously studied Li-Li symmetrical cells, we also annealed the Li anode cycled at ~0.75 mA cm^{-2} in the Li-S battery at a temperature of ~70°C for ~3 days in an Ar environment. The relatively smooth morphology of the thermally annealed Li foil (fig. S17F) closely matches the foil (fig. S17E) that was tested at a current density of ~9.0 mA cm^{-2} in the Li-S cell. EIS analysis (fig. S18 and tables S1 and S2) indicated that even after only 50 cycles, the electrolyte and interface resistance increased greatly when the Li-S cell was cycled at ~0.75 mA cm^{-2} as compared with ~9.0 mA cm^{-2}, which is consistent with dendrite healing at the high current density. The dendrite healing was also verified by means of cross-section SEM of the Li electrode (fig. S19).

We further investigated whether the Li-S battery could operate in short bursts at high current densities (with the purpose of healing the dendritic projections) and then revert back to operation at normal (low) current densities. This is demonstrated in Fig. 3A, indicating that periodic operation at high current densities (~9 mA cm^{-2}) for a limited duration is sufficient to heal the dendrites and substantially improve the CE (Fig. 3B) and to a lesser degree the capacity retention (fig. S20) performance of the battery under regular (~0.75 mA cm^{-2} current density) operating conditions. The gradual capacity fade over extended cycling (300 charge-discharge steps) observed in Fig. 3A was caused by dissolution of intermediate Li polysulfides into the electrolyte on the cathode (S) side. Such

capacity fade is typical of Li-S batteries without polysulfide immobilizers (*19*) or specialized barrier coatings (*20*) to prevent polysulfide dissolution.

We performed post-cycling characterization of the Li metal electrodes and the membrane separators used in these tests. SEM imaging of the Li anode surface at the end of the third healing step in Fig. 3A (after the 360th charge-discharge cycle) is shown in Fig. 3E. The results indicate a healed (relatively smooth) surface morphology without any sharp dendritic features. It is improbable that such a relatively flat surface could penetrate and punch through the separator membrane. This was confirmed with the optical microscopy images (Fig. 3, C and D) of the separator membrane in the post-cycled state. The membrane from the cell that was cycled at ~0.75 mA cm^{-2} for 250 charge-discharge steps without any healing treatment showed the presence of prominent dendritic Li deposits that were impregnated into the separator (Fig. 3C). Such Li metal deposits will eventually electrically short the Li-S battery (fig. S21). By contrast, the separator taken from the Li-S cell that was exposed to periodic doses of healing treatment (at ~9 mA cm^{-2}) (Fig. 3A) showed no indication (Fig. 3D) of such Li metal deposits even after extended cycling for 360 charge-discharge steps.

An important practical consideration for the healing strategy presented here is the time taken for the healing to be complete. When high current density is applied, there is an initial drop (fig. S22A) in the CE as the dendritic surface and SEI reconstructs. Subsequently, as the surface smoothens (fig. S22B) and stabilizes, the CE rises back up to a high value. The healing time can be inferred from the time (~2 to 3 hours in fig. S22A) that it takes for the CE to recover back to a high value after the initial dip. This healing time is expected to vary as a function of the applied current density. In addition to duration of healing, the frequency at which the healing treatment is repeated is also an important parameter, especially for minimizing the drying of the electrolyte. Our results showcase a promising path toward the effective deployment of Li metal electrodes in rechargeable batteries.

REFERENCES AND NOTES

1. P. Simon, Y. Gogotsi, B. Dunn, *Science* **343**, 1210–1211 (2014).
2. E. M. Lotfabad *et al.*, *ACS Nano* **8**, 7115–7129 (2014).
3. J. M. Tarascon, M. Armand, *Nature* **414**, 359–367 (2001).
4. W. Xu *et al.*, *Energy Environ. Sci.* **7**, 513–537 (2014).
5. H. Kim *et al.*, *Chem. Soc. Rev.* **42**, 9011–9034 (2013).
6. D. Aurbach, E. Zinigrad, Y. Cohen, H. Teller, *Solid State Ion.* **148**, 405–416 (2002).
7. Y. Lu, Z. Tu, L. A. Archer, *Nat. Mater.* **13**, 961–969 (2014).
8. A. Kushima *et al.*, *Nano Energy* **32**, 271–279 (2017).
9. A. Aryanfar *et al.*, *J. Phys. Chem. Lett.* **5**, 1721–1726 (2014).
10. A. Pei, G. Zheng, F. Shi, Y. Li, Y. Cui, *Nano Lett.* **17**, 1132–1139 (2017).
11. M. Ishikawa, H. Kawasaki, N. Yoshimoto, M. Morita, *J. Power Sources* **146**, 199–203 (2005).
12. T. J. Richardson, G. Chen, *J. Power Sources* **174**, 810–812 (2007).
13. L. Gireaud, S. Grugeon, S. Laruelle, B. Yrieix, J. M. Tarascon, *Electrochem. Commun.* **8**, 1639–1649 (2006).
14. G. Zheng *et al.*, *Nat. Nanotechnol.* **9**, 618–623 (2014).
15. C. P. Yang, Y. X. Yin, S. F. Zhang, N. W. Li, Y. G. Guo, *Nat. Commun.* **6**, 8058 (2015).
16. R. Mukherjee *et al.*, *Nat. Commun.* **5**, 3710 (2014).
17. Y. Liu *et al.*, *Nat. Energy* **2**, 17083 (2017).
18. Materials and methods are available as supplementary materials.
19. J. Gao *et al.*, *Nano Lett.* **16**, 3780–3787 (2016).
20. G. Zhou *et al.*, *Adv. Mater.* **27**, 641–647 (2015).

ACKNOWLEDGMENTS

Funding: N.K. acknowledges support from the U.S. National Science Foundation (awards 1234641, 1435783, 1510828, and 1608171) and the John A. Clark and Edward T. Crossan endowed Chair Professorship at the Rensselaer Polytechnic Institute. J.S. acknowledges the support from U.S. National Science Foundation under award CMMI 1635520. **Author contributions:** L.L. performed electrochemical testing and materials characterization; Y.W. contributed to interpreting the healing mechanism; L.L. and N.K. performed modeling of dendrite nucleation; S.B., N.K., and Y.S. carried out MD simulations; L.L., Y.W., Z.C., and J.S. carried out in situ optical imaging; L.L., P.H., and B.W. carried out x-ray photoelectron spectroscopy and XRD analysis; N.K. and S.N. carried out computational thermal modeling; and L.L., S.B., Y.S., S.N., and N.K. wrote the paper. The project was directed and supervised by N.K. **Competing interests:** Authors have no competing interests. **Data and materials availability:** All data are available in the manuscript or the supplementary materials.

SUPPLEMENTARY MATERIALS

www.sciencemag.org/content/359/6383/1513/suppl/DC1
Materials and Methods
Supplementary Text
Figs. S1 to S22
Tables S1 and S2
References (*21–25*)

5 September 2017; resubmitted 2 November 2017
Accepted 21 February 2018
10.1126/science.aap8787

Self-heating–induced healing of lithium dendrites

Lu Li, Swastik Basu, Yiping Wang, Zhizhong Chen, Prateek Hundekar, Baiwei Wang, Jian Shi, Yunfeng Shi, Shankar Narayanan and Nikhil Koratkar

Science **359** (6383), 1513-1516.
DOI: 10.1126/science.aap8787

Healing away the dendrites

The formation of lithium dendrites during charge-discharge cycles limits the development of lithium metal batteries, because the dendrites can cause electrical shorting of the cells. A number of tricks have been used to try to prevent dendrite formation. Li *et al.* took the opposite approach (see the Perspective by Mukhopadhyay and Jangid). They operated their cells at higher current densities, under which one would expect dendrites to form owing to the higher nucleation rates. However, under these conditions, the dendrites that started to form heated up and annealed, leading to their disappearance.

Science, this issue p. 1513; see also p. 1463